FADAC-OFDM: Frequency-Asynchronous Distributed Alamouti-Coded OFDM

Bong-seok Kim, *Member, IEEE* and Kwonhue Choi†, *Senior Member, IEEE*

***Abstract*—We propose frequency-asynchronous distributed Alamouti coded OFDM (orthogonal frequency division multiplexing), named FADAC-OFDM in short. The proposed scheme (FADAC-OFDM) effectively mitigates the inter-carrier interference (ICI) due to frequency offset (FO) between two distributed antennas. The transmitter side of the proposed scheme transmits each of the two subslots in Alamouti code through two remote subcarriers symmetric to the center frequency, and is referred to as space frequency reversal schemes by Xia [1] or Choi [3]. The receiver side of the proposed scheme is significantly different from the conventional scheme or the scheme proposed in reference [1] in that it performs two discrete fourier transform (DFT), each of which is synchronized to each transmit antenna's carrier frequency. The decision variables are generated by performing a simple linear combining with the same complexity as that of the conventional Alamouti code. The derivation shows that in flat fading channels, the dominant ICI components due to FO cancel each other during the combining process. The proposed scheme achieves almost the same performance as the ideal Alamouti scheme, even with large FO. To use this ICI self-cancellation property for selective fading channels or in cases with timing offset between two transmit antennas, the total subcarriers are divided into several subblocks and the proposed scheme is applied to each subblock. For mildly selective channels or cases with practically small timing offset, the proposed scheme achieves significantly improved performance compared to the conventional space frequency Alamouti coded OFDM.**

***Index Terms*—OFDM, Alamouti, Frequency Offset, Inter Carrier Interference, Distributed Antennas, Cooperative Communications.**

I. Introduction

Recently, several studies on Alamouti coded OFDM for cooperative systems have been reported. One of the main challenging issues in this area is to mitigate self interference due to the frequency offset (FO) between the distributed transmit antennas [1]–[8]. The FO between the transmitters destroys the designed Alamouti code property and degrades the performance. This is more significant in OFDM-modulated Alamouti code because the FO in the OFDM signals generate inter-carrier interference (ICI).

As one of the most promising among the various approaches in [1]–[8], so called 'frequency reversal schemes' have been recently proposed for Alamouti coded distributed OFDM in [1]–[3]. The transmit sides of these schemes share a common structure in that each of the two subslots in Alamouti code are transmitted through two remote subcarriers symmetrical around the center frequency. However, the motivations are quite different. In the previous study [1], frequency reversal scheme was employed to achieve a block-Alamouti-liked structure and ignore the interferences from the conjugate version of the data symbol vector. On the other hand, Li and Xia [2] and Choi [3] used the frequency reversal schemes to exploit the interference self-cancellation effect during simple linear combining at the receiver.

More specifically in [1], ICI is mitigated using linear receivers, such as ZF (zero forcing) and MMSE (minimum mean square error). However, large dimension channel matrix inversion is required because channel inversion is performed across the subcarriers. In addition, null data symbols are transmitted at some subcarrier positions where the major interference terms originate from, resulting in inevitable data rate loss. Under large FO conditions, performance degradation is unavoidable, even though the number of null subcarriers increases. Li and Xia [2] proposed an Alamouti coded OFDM scheme that is robust to both FO and timing offsets. The data rate, however, is less than half that of the conventional scheme. Moreover, they consider real-valued channel fading and the desired performance is achieved only for the specific regions of FO. In our previous work [3], we proposed a scheme which completely cancels the ICI with full data rate using a frequency reversal scheme over two consecutive OFDM symbols. This scheme has a drawback that the FO feedback information is needed to cancel the phase drift between two consecutive OFDM symbols due to FO. Another common limitation of the schemes in [1]–[3] is that the flat fading channel was considered and the applicability to the selective fading channel was not addressed. In [4], ICI cancellation scheme was proposed for the selective fading channel. Similarly to [3], the scheme in [4] performs two DFT operations which are separately synchronized to each transmit antenna's carrier frequency before Alamouti code combining. Unlike the previous schemes in [1]–[3], the scheme in [4] performs additional cancellation steps to the combined symbols. Although it achieves substantial ICI reduction in the small FO range, the severe performance degradation is still observed in the large FO range. Moreover, it needs the computational complexity overhead for the additional cancellation operation.

In this paper, we propose a frequency offset-tolerant Alamouti coded OFDM for frequency asynchronous distributed antenna systems, named in short FADAC-OFDM (frequency-asynchronous distributed Alamouti coded OFDM). The pro-

The authors are with the Department of Information and Communication Engineering, Yeungnam University, Korea 712-749. †Corresponding author (e-mail: gonew@yu.ac.kr).
"This research was supported by Basic Science Research Program through the National Research Foundation of Korea(NRF) funded by the Ministry of Education, Science and Technology(2012R1A1A4A01015628)"

posed system (FADAC-OFDM) employs frequency reversal scheme at the transmitter side similar to those in [1]–[3]. Differently from those in [1] and [2], the proposed scheme detects the symbols by performing simple linear combining after two separate DFT operations with local carriers synchronized to each transmit antenna. We show that the proposed detection for frequency reversal scheme inherently cancels major ICI terms from the neighboring subcarriers. The receiver complexity of the proposed scheme is quite simple compared to that by Wang and Xia [1] despite the two DFT operations because it does not require a large dimension matrix manipulation, such as matrix inversion. The formulation in Section V shows that the scheme by Wang and Xia requires roughly $N/2$ (N= number of subcarriers) times larger computation complexity than that of the proposed scheme. In addition, data rate loss of the proposed scheme is much smaller than that of [1]. Compared to Choi's scheme [3], the proposed scheme is based on space-frequency Alamouti code, where data symbol is encoded using two different subcarriers of one OFDM symbol, and there is no phase drift problem. Therefore, the proposed scheme does not require any feedback for pre-compensation in the transmitter. In the implementation view point, this is a remarkable benefit over Choi's scheme [3].

The structure of the paper is as follows. In Section II, we introduce the proposed scheme. In Section III, we mathematically show how it substantially cancels the ICI by simple linear combining for flat fading channel and then provide an extension of the proposed scheme for selective fading channels or practical cases with timing offset between two transmit antennas. Finally in Section IV, the simulation results for various cases are provided.

II. Channel model and the proposed Alamouti coded OFDM scheme

A. Channel model and notations

This paper considers the distributed antenna system that is composed of two TX (transmit) antennas and one RX (receive) antenna [1]–[5]. In each TX antenna, OFDM modulated signals are transmitted. The channel fading coefficients of the kth subcarrier from TX antennas A and B, are denoted by $H_k^{(A)}$ and $H_k^{(B)}$, respectively. We assume that $H_k^{(A)}$ and $H_k^{(B)}$ are independent and follow zero mean, unit variance complex Gaussian distribution. The practical distributed antenna system was considered where there is some mismatch between the received carrier frequency $f_c^{(A)}$ from the TX antenna A and the received carrier frequency $f_c^{(B)}$ from the TX antenna B [1]–[3]. At first, the OFDM symbol duration T is assumed to be sufficiently enlarged and the symbol timing alignment performs well enough to ignore the symbol timing offset between the received signals from the two TX antennas [10]. In the latter part of Section III, the channel model with a practical tiny timing offset is also considered and the modified version of the proposed scheme is provided. The number of total subcarriers is denoted by N. Therefore, N Alamouti−encoded data symbols are transmitted in space (2 antennas)−frequency (N subcarriers) domain. The lth data symbol is denoted as x_l. Then, Alamouti code pairs of x_l and x_{l+1} are given as $-x_{l+1}^*$ and x_l^*, respectively [11]. The Alamouti code symbols at the kth subcarrier from TX antennas A and B, are denoted as $X_k^{(A)}$ and $X_k^{(B)}$, respectively.

B. The space frequency reversal Alamouti coded OFDM structure

Figs. 1 and 2 show the structures of the conventional space frequency Alamouti coded OFDM and the space frequency reversal Alamouti coded OFDM, respectively. In the conventional scheme, the Alamouti code pairs are mapped to the neighboring subcarriers, as shown in Fig. 1 [9], i.e., $X_k^{(A)}$ and $X_k^{(B)}$ are set to

$$X_k^{(A)} = \begin{cases} x_k & \text{if } k \text{ is odd,} \\ -x_k^* & \text{if } k \text{ is even,} \end{cases} \tag{1}$$

$$X_k^{(B)} = \begin{cases} x_{k+1} & \text{if } k \text{ is odd,} \\ x_{k-1}^* & \text{if } k \text{ is even.} \end{cases} \tag{2}$$

frequency / space	Subcarrier index, k						
	1	2	3	4	⋯	$N-1$	N
$X_k^{(A)}$	x_1	$-x_2^*$	x_3	$-x_4^*$	⋯	x_{N-1}	$-x_N^*$
$X_k^{(B)}$	x_2	x_1^*	x_4	x_3^*	⋯	x_N	x_{N-1}^*

Alamouti code symbol pairs

Fig. 1. Structure of the conventional space frequency Alamouti coded OFDM.

frequency / space	Subcarrier index, k						
	1	2	3	⋯	$N-2$	$N-1$	N
$X_k^{(A)}$	x_1	x_3	x_5	…	$-x_6^*$	$-x_4^*$	$-x_2^*$
$X_k^{(B)}$	x_2	x_4	x_6	…	x_5^*	x_3^*	x_1^*

Alamouti code symbol pairs

Fig. 2. Structure of the space frequency reversal Alamouti coded OFDM.

On the other hand, the space frequency reversal scheme maps the Alamouti code pair into a mirror image, as shown in Fig. 2. Therefore, $X_k^{(A)}$ and $X_k^{(B)}$ are set to

$$X_k^{(A)} = \begin{cases} x_{2k-1} & \text{for } 1 \le k \le N/2, \\ -x_{2(N-k+1)}^* & \text{for } N/2+1 \le k \le N, \end{cases} \tag{3}$$

$$X_k^{(B)} = \begin{cases} x_{2k} & \text{for } 1 \le k \le N/2, \\ x_{2(N-k)+1}^* & \text{for } N/2+1 \le k \le N. \end{cases} \tag{4}$$

The proposed system employs frequency reversal scheme at the transmitter side.

C. The receiver algorithm of the proposed scheme

This section explains the receiver algorithm of the proposed scheme. In the proposed scheme, the received signal undergoes two DFT operations with local carrier frequencies synchronized to the received signal from each TX antenna. The first one is performed with the local carrier synchronized to $f_c^{(A)}$ and the other one is performed with the local carrier synchronized to $f_c^{(B)}$. If the receiver synchronizes its local carrier frequency to $f_c^{(A)}$, the DFT output at the subcarrier k denoted by $R_k^{(A)}$ can be expressed as

$$\begin{aligned} R_k^{(A)} &= H_k^{(A)} X_k^{(A)} + \sum_{m=1}^{N} Q(m+\varepsilon-k) H_m^{(B)} X_m^{(B)} \\ &+ n_k^{(A)}, \text{for } \ 1 \le k \le N/2, \end{aligned} \tag{5}$$

$$\begin{aligned} R_{N-k+1}^{(A)} &= H_{N-k+1}^{(A)} X_{N-k+1}^{(A)} \\ &+ \sum_{m=1}^{N} Q(m+\varepsilon-(N-k+1)) H_m^{(B)} X_m^{(B)} \\ &+ n_{N-k+1}^{(A)}, \text{for } \ 1 \le k \le N/2 \end{aligned} \tag{6}$$

where $n_k^{(A)}$ and $n_{N-k+1}^{(A)}$ are DFT output of the AWGN terms, and ε is a normalized frequency offset between two TX antennas, i.e. $\varepsilon = \left(f_c^{(B)} - f_c^{(A)}\right)/f_\Delta$ and f_Δ $(= 1/T)$ is the subcarrier spacing. The ICI coefficient $Q(x)$ is given as follows [12] :

$$Q(x) = \frac{\sin(\pi x)}{N \sin((\pi/N)x)} e^{j\pi(1-1/N)x}, \tag{7}$$

which satisfies the Hermitian symmetry with respect to the frequency difference x, that is $Q(x) = Q^*(-x)$.

Similarly, if the receiver synchronizes its local carrier frequency to $f_c^{(B)}$, the DFT output at the subcarrier k, denoted by $R_k^{(B)}$ is expressed as

$$\begin{aligned} R_k^{(B)} = H_k^{(B)} X_k^{(B)} + \sum_{m=1}^{N} Q(m-\varepsilon-k) H_m^{(A)} X_m^{(A)} + n_k^{(B)}, \\ \text{for } \ 1 \le k \le N/2, \end{aligned} \tag{8}$$

$$\begin{aligned} R_{N-k+1}^{(B)} &= H_{N-k+1}^{(B)} X_{N-k+1}^{(B)} \\ &+ \sum_{m=1}^{N} Q(m-\varepsilon-(N-k+1)) H_m^{(A)} X_m^{(A)} \\ &+ n_{N-k+1}^{(B)}, \text{for } \ 1 \le k \le N/2 \end{aligned} \tag{9}$$

where $n_k^{(B)}$ and $n_{N-k+1}^{(B)}$ are the DFT output of AWGN terms.

In the proposed scheme, D_{2k-1} and D_{2k}, which denote the decision variables corresponding to x_{2k-1} and x_{2k} are generated by combining two pairs of DFT outputs, respectively, as follows :

$$D_{2k-1} = H_k^{*(A)} R_k^{(A)} + H_{N-k+1}^{(B)} R_{N-k+1}^{*(B)} \tag{10}$$

$$D_{2k} = H_k^{*(B)} R_k^{(B)} - H_{N-k+1}^{(A)} R_{N-k+1}^{*(A)}. \tag{11}$$

From (10) and (11), we note that similar to the conventional detection of space frequency Alamouti code without FO, only two samples of DFT outputs are involved to generate decision variables, which was not the case in the scheme of [1]. Owing to this simple detection, the overall complexity of the proposed scheme is much smaller than that of the scheme in [1] despite one more DFT operation.

III. ICI SELF-CANCELLATION IN THE DECISION VARIABLES OF THE PROPOSED SCHEME

This section shows that the major parts of the ICI components are self-cancelled during the combining process of the proposed scheme.

A. Flat fading channel

First, the flat fading channel is considered. Therefore, $H_k^{(A)}$ and $H_k^{(B)}$ are changed to $H^{(A)}$ and $H^{(B)}$, respectively. The next subsection extends the subsequent analysis to the frequency selective fading channel.

We follow the derivation frame in our previous work [3] but the derivation details and results are significantly differ each other owing to different Alamouti code structures. Substituting (5) and (9) into (10) with $X_k^{(A)}$ and $X_k^{(B)}$ replaced by (3) and (4), results in D_{2k-1} as the summation of the signal term d_{2k-1} and four interference terms $I_{2k-1,1}$, $I_{2k-1,2}$, $I_{2k-1,3}$ and $I_{2k-1,4}$ as follows :

$$\begin{aligned} D_{2k-1} = & \underbrace{\left(\left|H^{(A)}\right|^2 + \left|H^{(B)}\right|^2\right) x_{2k-1}}_{\triangleq d_{2k-1}} \\ & + \underbrace{H^{*(A)} H^{(B)} \sum_{m=1}^{N/2} Q\left(m+\varepsilon-k\right) x_{2m}}_{\triangleq I_{2k-1,1}} \\ & + \underbrace{H^{*(A)} H^{(B)} \sum_{m=N/2+1}^{N} Q\left(m+\varepsilon-k\right) x_{2(N-m)+1}^*}_{\triangleq I_{2k-1,2}} \\ & + \underbrace{H^{*(A)} H^{(B)} \sum_{m=1}^{N/2} Q^*(m-\varepsilon-(N-k+1)) x_{2m-1}^*}_{\triangleq I_{2k-1,3}} \\ & + \underbrace{H^{*(A)} H^{(B)} \sum_{m=N/2+1}^{N} Q^*(m-\varepsilon-(N-k+1))(-x_{2(N-m+1)}^*)^*}_{\triangleq I_{2k-1,4}} \end{aligned} \tag{12}$$

where the subscript index $2k-1$ in the newly defined terms beneath the underlines implies that the decision variable of the $(2k-1)$-th data symbol x_{2k-1} is under consideration. The AWGN terms are not included because their distributions after combining are the same as those of the conventional Alamouti coded OFDM without frequency offset [3].

The terms, $I_{2k-1,1}$ and $I_{2k-1,4}$ denote the ICI from the subcarriers of the half-side where the desired subcarrier belongs to, whereas $I_{2k-1,2}$ and $I_{2k-1,3}$ denote the ICI from the other half-side. Therefore, we can conjecture that $I_{2k-1,1}$ and $I_{2k-1,4}$ are the dominant ICI terms over $I_{2k-1,2}$ and $I_{2k-1,3}$.

In order to theoretically check this conjecture, let us calculate and compare the variances of four ICI terms i.e., $I_{2k-1,1}$, $I_{2k-1,4}$, $I_{2k-1,2}$ and $I_{2k-1,3}$. We first calculate the signal power-normalized variance of $I_{2k-1,1}$ denoted by $\sigma^2_{2k-1,1}$ as follows:

$$\sigma^2_{2k-1,1} \triangleq \mathrm{E}\left[\frac{|I_{2k-1,1}|^2}{|d_{2k-1}|^2}\right]$$
$$= \mathrm{E}\left[\frac{\left|H^{(A)}\right|^2\left|H^{(B)}\right|^2\left|\sum_{m=1}^{N/2} Q(m+\varepsilon-k)x^*_{2m}\right|^2}{\left|\left|H^{(A)}\right|^2+\left|H^{(B)}\right|^2\right|^2|x_{2k-1}|^2}\right]$$
$$= \mathrm{E}\left[\frac{\left|H^{(A)}\right|^2\left|H^{(B)}\right|^2}{\left|\left|H^{(A)}\right|^2+\left|H^{(B)}\right|^2\right|^2}\right]\mathrm{E}\left[\frac{\left|\sum_{m=1}^{N/2} Q(m+\varepsilon-k)x^*_{2m}\right|^2}{|x_{2k-1}|^2}\right] \quad (13)$$

where $\mathrm{E}[\cdot]$ is the expectation operator. The magnitude squares of complex Gaussian variables with unit variance, i.e., $\left|H^{(A)}\right|^2$ and $\left|H^{(B)}\right|^2$ follow exponential distributions with unit mean. Hence, the first expectation term in (13) is calculated as follows (see Appendix for detailed derivation) :

$$\mathrm{E}\left[\frac{\left|H^{(A)}\right|^2\left|H^{(B)}\right|^2}{\left|\left|H^{(A)}\right|^2+\left|H^{(B)}\right|^2\right|^2}\right] = \int_0^\infty\int_0^\infty e^{-x}e^{-y}\frac{xy}{(x+y)^2}\mathrm{d}x\mathrm{d}y$$
$$= 1/6. \quad (14)$$

Assuming that the data symbols have the constant magnitude of C, the second expectation in (13) is derived as

$$\mathrm{E}\left[\left|\sum_{m=1}^{N/2} Q(m+\varepsilon-k)x^*_{2m}\right|^2/|x_{2k-1}|^2\right]$$
$$= 1/C\sum_{m=1}^{N/2}\sum_{l=1}^{N/2} Q(m+\varepsilon-k)Q^*(l+\varepsilon-k)\mathrm{E}\left[x^*_{2m}x_{2l}\right]. \quad (15)$$

With another assumption that data symbols are independent each other without loss of generality, the term $\mathrm{E}[x^*_{2m}x_{2l}]$ is expressed as

$$\mathrm{E}\left[x^*_{2m}x_{2l}\right] = \begin{cases} C, & m=l \\ 0, & \text{otherwise.}\end{cases} \quad (16)$$

Substituting (16) into (15), (15) is written as

$$\mathrm{E}\left[\left|\sum_{m=1}^{N/2} Q(m+\varepsilon-k)x^*_{2m}\right|^2/|x_{2k-1}|^2\right]$$
$$= 1/C\sum_{m=1}^{N/2}|Q(m+\varepsilon-k)|^2\times C$$
$$= \sum_{m=1}^{N/2}|Q(m+\varepsilon-k)|^2. \quad (17)$$

Consequently, using (14) and (17), (13) is derived as

$$\sigma^2_{2k-1,1} = 1/6\sum_{m=1}^{N/2}|Q(m+\varepsilon-k)|^2. \quad (18)$$

Similarly, $\sigma^2_{2k-1,2}$, $\sigma^2_{2k-1,3}$ and $\sigma^2_{2k-1,4}$ are derived as

$$\sigma^2_{2k-1,2} = 1/6\sum_{m=N/2+1}^{N}|Q(m+\varepsilon-k)|^2, \quad (19)$$

$$\sigma^2_{2k-1,3} = 1/6\sum_{m=1}^{N/2}|Q(m-\varepsilon-(N-k+1))|^2, \quad (20)$$

$$\sigma^2_{2k-1,4} = 1/6\sum_{m=N/2+1}^{N}|Q(m-\varepsilon-(N-k+1))|^2. \quad (21)$$

In Fig. 3, $\sigma^2_{2k-1,1}$, $\sigma^2_{2k-1,2}$, $\sigma^2_{2k-1,3}$ and $\sigma^2_{2k-1,4}$ are plotted for $N=64$ and several εs. As expected, $I_{2k-1,1}$ and $I_{2k-1,4}$ are the major parts of ICI components as they are significantly larger than $I_{2k-1,2}$ and $I_{2k-1,3}$.

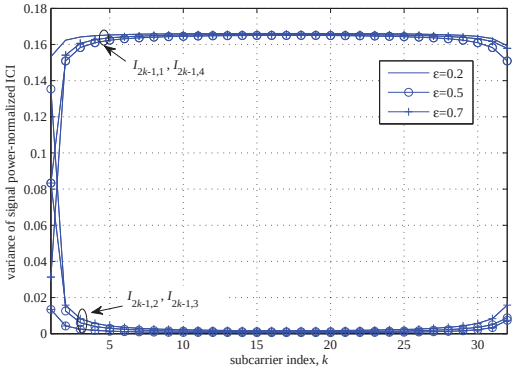

Fig. 3. The variances of $I_{2k-1,1}$, $I_{2k-1,2}$, $I_{2k-1,3}$ and $I_{2k-1,4}$ with $N=64$ and several ε.

For $I_{2k-1,4}$ in (12), a new indexing variable, $m' = N-m+1$ is used to rearrange $N/2+1 \le m \le N$ in reverse order. From (7), $Q(x) = Q^*(-x)$ and thus $Q^*(-(m-\varepsilon-k)) = Q(m+\varepsilon-k)$. Therefore, $I_{2k-1,4}$ can be rewritten as

$$I_{2k-1,4}$$
$$= H^{*(A)}H^{(B)}\sum_{m'=1}^{N/2} Q^*(N-m'+1-\varepsilon-(N-k+1))(-x^*_{2m'})^*$$
$$= -H^{*(A)}H^{(B)}\sum_{m=1}^{N/2} Q^*(-m-\varepsilon+k)x_{2m}$$
$$= -H^{*(A)}H^{(B)}\sum_{m=1}^{N/2} Q(m+\varepsilon-k)x_{2m}$$
$$= -I_{2k-1,1}. \quad (22)$$

From (22), it is remarkable that $I_{2k-1,1}$ and $I_{2k-1,4}$ in (12) cancel each other. By cancelling $I_{2k-1,1}$ and $I_{2k-1,4}$, which are dominant ICI terms, the performance degradation due to ICI can be substantially ameliorated. This feature of the proposed scheme is the most distinguishable from the existing methods in [1], [2].

Another similar calculation can show that $I_{2k-1,2} = I_{2k-1,3}$, and (12) can be rewritten as

$$D_{2k-1} = \underbrace{\left(\left|H^{(A)}\right|^2 + \left|H^{(B)}\right|^2\right) x_{2k-1}}_{=d_{2k-1}} + \underbrace{2H^{*(A)}H^{(B)}\left(\sum_{m=N/2+1}^{N} Q(m+\varepsilon-k)x^*_{2(N-m)+1}\right)}_{=2I_{2k-1,2}}. \quad (23)$$

Using a similar calculation, D_{2k} is represented without difficulty as

$$D_{2k} = \underbrace{\left(\left|H^{(A)}\right|^2 + \left|H^{(B)}\right|^2\right) x_{2k}}_{\triangleq d_{2k}} + \underbrace{2H^{(A)}H^{*(B)}\left(\sum_{m=N/2+1}^{N} Q\left(m-\varepsilon-k\right) x^*_{2(N-m+1)}\right)}_{\triangleq 2I_{2k,2}}. \quad (24)$$

Comparing (23) and (24) to the decision variables in [3], we note the difference that the proposed scheme has the residual ICI terms whereas the scheme in [3] perfectly cancels ICI. This comes from the difference in Alamouti code structure that the proposed scheme transmits Alamouti code symbol pairs in the same OFDM symbol while the scheme in [3] transmits Alamouti code symbol pairs over two OFDM symbols. On the other hand, this difference also results in remarkable benefit of the proposed scheme over the scheme in [3], i.e., no need for feedback information to the TX. Remind the critical limitation of the scheme in [3] that the perfect ICI cancellation is impossible without FO feedback information to the TX. In addition to no feedback requirement of the proposed scheme, the degradation due to the residual ICI is shown to be negligible in the following paragraph.

Denote the variances of the signal-normalized residual ICI terms in D_{2k-1} and D_{2k} as v_{2k-1} and v_{2k}, respectively, they then are expressed as follows :

$$v_{2k-1} = \mathrm{E}\left[\frac{\left|2I_{2k-1,2}\right|^2}{\left|d_{2k-1}\right|^2}\right] = 4\sigma^2_{2k-1,2} = \frac{2}{3}\sum_{m=N/2+1}^{N}|Q(m+\varepsilon-k)|^2, \quad (25)$$

$$v_{2k} = \mathrm{E}\left[\frac{\left|2I_{2k,2}\right|^2}{\left|d_{2k}\right|^2}\right] = 4\sigma^2_{2k,2} = \frac{2}{3}\sum_{m=N/2+1}^{N}|Q(m-\varepsilon-k)|^2. \quad (26)$$

For nonconstant magnitude modulations such as QAM (quadrature amplitude modulation), the term $|x_{2k-1}|^2$ is not a constant and thus, v_{2k-1} and v_{2k} are given as

$$v_{2k-1} = \frac{2}{3}\mathrm{E}\left[\frac{\sum_{m=N/2+1}^{N}|Q(m+\varepsilon-k)|^2|x_{2(N-m)+1}|^2}{|x_{2k-1}|^2}\right] = \frac{2}{3}\sum_{m=N/2+1}^{N}|Q(m+\varepsilon-k)|^2\mathrm{E}\left[\frac{|x_{2(N-m)+1}|^2}{|x_{2k-1}|^2}\right], \quad (27)$$

$$v_{2k} = \frac{2}{3}\sum_{m=N/2+1}^{N}|Q(m-\varepsilon-k)|^2\mathrm{E}\left[\frac{|x_{2(N-m+1)}|^2}{|x_{2k}|^2}\right], \quad (28)$$

where the term $\mathrm{E}\left[\frac{|x_{2(N-m)+1}|^2}{|x_{2k-1}|^2}\right]$ in (27) is written as

$$\mathrm{E}\left[\frac{|x_{2(N-m)+1}|^2}{|x_{2k-1}|^2}\right] = \begin{cases} 1 & \text{if} \quad m = N-k+1 \\ \mathrm{E}\left[|x_{2(N-m)+1}|^2\right] \times \mathrm{E}\left[1/|x_{2k-1}|^2\right] & \text{else.} \end{cases} \quad (29)$$

For QAM with the symbol size M, the term $\mathrm{E}\left[|x_{2(N-m)+1}|^2\right] \times \mathrm{E}\left[1/|x_{2k-1}|^2\right]$ is calculated as

$$\mathrm{E}\left[|x_{2(N-m)+1}|^2\right] \times \mathrm{E}\left[1/|x_{2k-1}|^2\right] = \frac{1}{M}\sum_{m=-\sqrt{M}/2}^{\sqrt{M}/2}\sum_{n=-\sqrt{M}/2}^{\sqrt{M}/2}|(2m-1)+j(2n-1)|^2 \times \frac{1}{M}\sum_{k=-\sqrt{M}/2}^{\sqrt{M}/2}\sum_{l=-\sqrt{M}/2}^{\sqrt{M}/2}\frac{1}{|(2k-1)+j(2l-1)|^2} = \frac{2(M-1)}{3}\cdot\frac{1}{M}\sum_{k=-\sqrt{M}/2}^{\sqrt{M}/2}\sum_{l=-\sqrt{M}/2}^{\sqrt{M}/2}\frac{1}{|(2k-1)+j(2l-1)|^2}. \quad (30)$$

Similarly, the expectation term in (28) is derived as follows:

$$\mathrm{E}\left[\frac{|x_{2(N-m+1)}|^2}{|x_{2k}|^2}\right] = \begin{cases} 1 & \text{if } m = N-k+1 \\ \frac{2(M-1)}{3M}\sum_{k=\frac{-\sqrt{M}}{2}}^{\frac{\sqrt{M}}{2}}\sum_{l=\frac{-\sqrt{M}}{2}}^{\frac{\sqrt{M}}{2}}\frac{1}{|(2k-1)+j(2l-1)|^2} & \text{else.} \end{cases} \quad (31)$$

Going through the finite number of summations in (27), (28), (30) and (31), v_{2k-1} and v_{2k} can be accurately obtained for different k and M.

Fig. 4 shows v_{2k-1} and v_{2k} according to the subcarrier index k for Binary Phase Shift Keying (BPSK) and 16 QAM when $N = 64$ and 4096, respectively. The subcarrier indices for the data symbols are limited to the left half band of the OFDM signal because the right half band corresponds to their frequency reversal space frequency Alamouti code symbol pairs. In the upper subplots, v_{2k-1} in the (25) and (27) and v_{2k}

in (26) and (28) are plotted for FO $\varepsilon = 0.5$ and the simulation results confirm the exactness of the derivation.

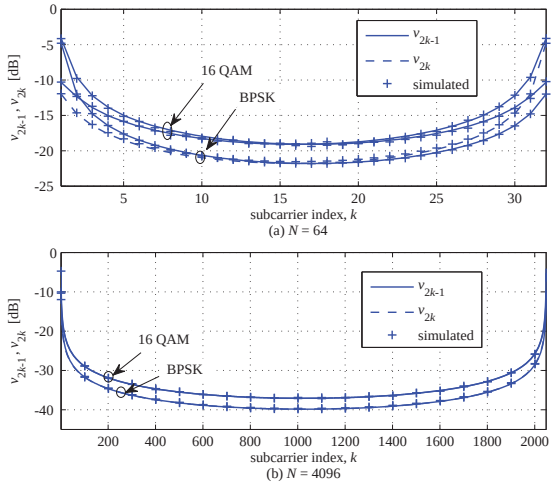

Fig. 4. v_{2k-1} and v_{2k} of x_{2k-1} and x_{2k} with BPSK and 16 QAM with $\varepsilon = 0.5$ when $N = 64$ and $N = 4096$.

It is notable that most of the data symbols off from half band edge ($k = 1$ and $N/2$[1]) have very small residual ICI power. Close to the half band edge, the residual ICI power increases and this holds irrespective of modulation symbol size M and the number of subcarriers N. This is because the ICI coefficient function $Q(x)$ in (25) $\sim$ (28) reaches its maximum at $x = 0$ and N. This result motivates us to transmit null-signal at the several subcarrier positions near the half band edge, which is beneficial in two aspects. First, the poor error rates near the half band edge due to large ICI power will not be included in the average error rate. Secondly, the subcarriers inducing the most dominant ICI are not transmitted. Comparing the cases with $N = 64$ and 4096, we note that the residual ICI power further decreases as N increases. This is because the portion of the subcarriers which are far from the half band edge increases as N increases. Meanwhile, comparing BPSK and 16 QAM, the overall residual ICI power increases for higher modulation symbol size. This is because the data symbol power ratios $\frac{|x_{2(N-m)+1}|^2}{|x_{2k}|^2}$ and $\frac{|x_{2(N-m+1)}|^2}{|x_{2k}|^2}$ in the expectation terms in (27) and (28) are possibly larger as M increases and consequently the overall expectation increases. This implies that the required number of null subcarriers for the desired performance depends on the symbol size M.

Fig. 5 shows the bit error rates (BER) of the proposed scheme with different Ms according to the number of null subcarriers N_u for the case when $N = 256$ and $\varepsilon = 0.1$, $\varepsilon = 0.2$ and 0.5. As for the null subcarrier positions, we transmit null data at $N_u/4$ right most and $N_u/4$ left most subcarriers of the left half block and simultaneously at their mirrored subcarrier positions in the right half band as well. This is equivalent to setting the data symbols $\left[x_1, x_2, \cdots, x_{\frac{N_u}{2}}\right]$ and $\left[x_{N-\frac{N_u}{2}+1}, x_{N-\frac{N_u}{2}+2}, \cdots, x_N\right]$ to all zeros in Fig. 2 and excluding them in the detection. As expected, the BER decreases and converges to ICI-free case as the number of null subcarriers increases. It's remarkable that the proposed scheme converges nearly ICI-free performance only with 4 null subcarriers for BPSK and QPSK modulations.

As the QAM symbol size M increases, the minimum required N_u increases for the convergence. From Fig. 5. (a) and Fig. 5. (b), we note that the minimum required N_u to get ICI-free BER for 256 QAM is somehow acceptable when FO falls in practical range [13], [14], i.e. 44 (17.2%) null subcarriers for $\varepsilon = 0.2$ and 8 (3.1%) null subcarriers for $\varepsilon = 0.1$. However, in the case of the worst FO $\varepsilon = 0.5$, roughly 100 (40%) null subcarriers are required for 256 QAM. This means that for large FO, very high order modulation such as 256 QAM does not go well with the proposed scheme. In order to explore an amicable aspect which relieves this very high order modulation problem, the minimum required N_us to get ICI-free BER for 256 QAM are obtained via simulations for several Ns and are listed in Table I. We note that the minimum required N_us are almost invariant to N and thus, the ratio of the minimum required N_u to N is inverse-proportional to N. For example, when N increases to 1024, only 4.3 % and 9.0 % null subcarriers are required for $\varepsilon = 0.2$ and $\varepsilon = 0.5$, respectively.

TABLE I
THE MINIMUM REQUIRED N_u WITH 256 QAM FOR ICI-FREE BER ACCORDING TO N AND ε.

N	The minimum required N_u for ICI-free BER		
	$\varepsilon = 0.1$	$\varepsilon = 0.2$	$\varepsilon = 0.5$
256	8 (3.1%)	44 (17.2%)	100 (39.1%)
512	8 (1.6%)	44 (8.6%)	96 (18.8%)
1024	8 (0.8%)	40 (4.3%)	92 (9.0%)
4096	8 (0.2%)	40 (1.1%)	92 (2.3%)

For the cases when N is not sufficiently large, we cannot avoid considerable bandwidth loss of the proposed scheme in the current structure for very high order modulation with large FO. To alleviate poor bandwidth efficiency due to a bunch of null subcarriers, we have to come up with a way to increase the portion of data subcarriers (decrease the portion of null subcarriers) without degrading error performance. This motivates us to consider a modification that we slightly downsize the very high order modulation zone and gradually decrease modulation symbol size approaching the half band edges instead of just filling there with null subcarriers. This is because the lower order modulation is more robust to the interference than the higher order modulation. Let us call this modification 'multiple modulation size mode (MMSM)'. Fig. 6 illustrates the modulation symbol size assignment of the MMSM in one OFDM signal where N_M denotes the assigned number of subcarriers with M-ary QAM symbols.

We extensively simulated various MMSMs with different combinations of modulation symbol size set when the maximum symbol size is 256. Depending on the modulation symbol size combinations, the error rate and the number of information bits per one OFDM signal differ and there exists a trade off between these two performance measure. Fig. 7 shows the error rate and the number of information bits

[1]Be sure that we are considering the *left* half band and thus the subcarrier indices for the left and right edges are 1 and $N/2$, respectively.

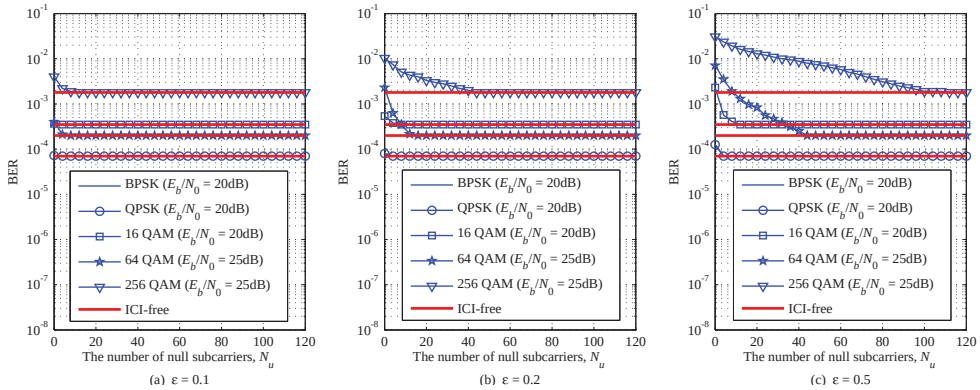

Fig. 5. BER curves according to the number of null subcarriers for several modulation symbol sizes of QAM.

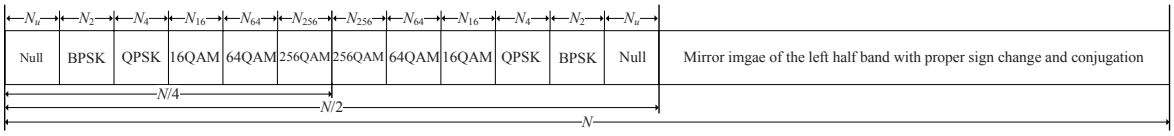

Fig. 6. Structure and assignment of multiple modulation size mode in one OFDM signal in frequency domain.

for several combinations of the modulation symbol size with $N = 256$, $\varepsilon = 0.5$ and $E_b/N_0 = 25$ dB. The MMSMs illustrated in Fig. 7 outperform the previous single modulation mode (a special case of MMSM with [N_u, N_2, N_4, N_{16}, N_{64}, N_{256}]=[25, 0, 0, 0, 0, 39]) not only in terms of the number of information bits but also in terms of error rate. For example, MMSM with [N_u, N_2, N_4, N_{16}, N_{64}, N_{256}]=[1, 1, 2, 7, 18, 35] achieves 34.9% improvement to the previous single modulation mode and this corresponds to 82.2% information bits of full 256 QAM mode without null subcarriers (a special case of MMSM with [N_u, N_2, N_4, N_{16}, N_{64}, N_{256}]=[0, 0, 0, 0, 0, 64]). Furthermore, the BER is lower than that of the previous single modulation mode[2]. This is because the portions of lower order modulations contribute to decrease the overall average BER.

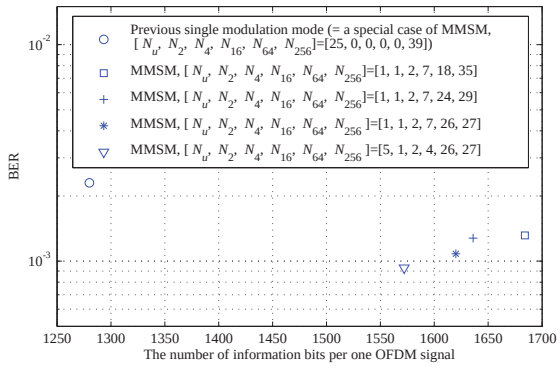

Fig. 7. BER and the number of information bits per one OFDM signal according to the modulation symbol size assignment with $N = 256$, $\varepsilon = 0.5$ and $E_b/N_0 = 25$ dB.

B. Extension to the frequency selective fading channel or cases with practical timing offset between TX antennas

This section extends the proposed scheme to be modified for the frequency selective fading channel or the case with practically tiny timing offset between the TX antennas. In the case when there is a timing offset between two TX antennas, and the receiver is time-synchronized to one of the TX antennas, the signal received from the other TX antenna undergoes nonconstant phase shifts for different subcarriers. When synchronized to somewhere between each TX antenna timing, both signals from each TX antenna undergo nonconstant phase shifts for different subcarriers. Consequently, the timing offset effectively makes even a flat fading channel appear like a selective fading channel [15]. From this point of view, we treat the case with timing offset between TX antennas as a special case of the selective fading channel.

In the frequency selective fading channel, the fading coefficient, $H_k^{(A)}$ and $H_k^{(B)}$, are not constant for different k. Therefore, $I_{2k-1,1}$ in (12) and $I_{2k-1,4}$ in (22) can be rewritten as

$$I_{2k-1,1} = H_k^{*(A)} \sum_{m=1}^{N/2} Q\left(m+\varepsilon-k\right) H_m^{(B)} x_{2m} \qquad (32)$$

$$I_{2k-1,4} = -H_k^{(B)} \sum_{m=1}^{N/2} Q\left(m+\varepsilon-k\right) H_{N-m+1}^{*(A)} x_{2m} \qquad (33)$$

from which, $I_{2k-1,1} \neq -I_{2k-1,4}$ because $H_m^{(B)}$ in (32) and $H_{N-m+1}^{*(A)}$ in (33) are not constant but vary according to m. Therefore, the ICI terms are not cancelled.

To exploit the ICI self-cancellation property of the proposed scheme even in these circumstances, the entire subcarriers are divided into several subblocks as shown in Fig. 8, and the proposed scheme is then applied to each subblock. In Fig. 8, n_c denotes the number of assigned subcarriers per subblock. Denoting the number of subblocks as N_b, n_c is equal to N/N_b. The fading coefficients within each subblock can be assumed to be approximately constant if the subblock size n_c is set properly in relation to the frequency selectivity. Let us call this modification of the proposed scheme as 'subblock mode'. The main difference of ICI in subblock mode compared to the 'single' block mode is that we have inter-block ICI. In order to assess this difference more analytically, we first revise (5)

[2]Be sure that ICI-free BER level differs depending on MMSM combination.

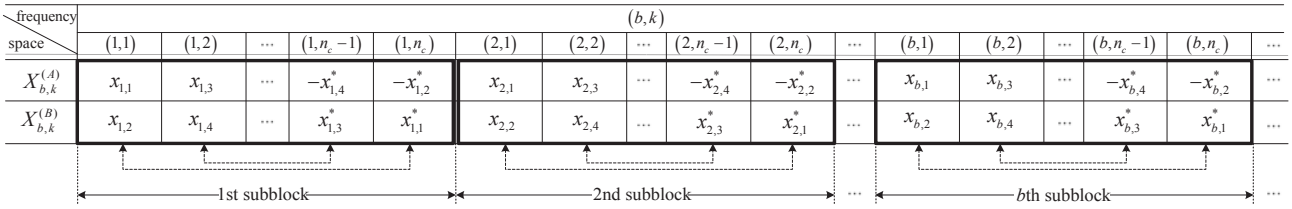

Fig. 8. Transmit structure of the proposed scheme for the frequency selective fading channel or the case with timing offset between transmit antennas.

and (8) properly to express DFT outputs of kth subcarrier of bth subblock of antenna A and B. They are denoted by $R_{b,k}^{(A)}$ and $R_{b,k}^{(B)}$, respectively and are expressed as

$$R_{b,k}^{(A)} = H_{b,k}^{(A)} X_{b,k}^{(A)} + \sum_{\beta=1}^{N_b} \sum_{m=1}^{n_c} Q\left((\beta-b)n_c + m + \varepsilon - k\right) H_{b,m}^{(B)} X_{b,m}^{(B)} \tag{34}$$

$$R_{b,k}^{(B)} = H_{b,k}^{(B)} X_{b,k}^{(B)} + \sum_{\beta=1}^{N_b} \sum_{m=1}^{n_c} Q\left((\beta-b)n_c + m - \varepsilon - k\right) H_{b,m}^{(A)} X_{b,m}^{(A)} \tag{35}$$

where $H_{b,k}^{(A)}$ and $H_{b,k}^{(B)}$ denote fading coefficient of kth subcarrier of bth subblock of antenna A and B, respectively. Also, $X_{b,k}^{(A)}$ and $X_{b,k}^{(B)}$ denote the Alamouti code symbols at the kth subcarrier from antenna A and B, respectively, and they are mapped according to Fig. 8 where (b,k) in the frequency axis denotes the index of the kth subcarrier of bth subblock and $x_{b,l}$ is the lth data symbol in bth subblock. We can write the decision variables for $x_{b,2k-1}$ and $x_{b,2k}$ by revising (10) and (11) as follows :

$$D_{b,2k-1} = H_{b,k}^{*(A)} R_{b,k}^{(A)} + H_{b,n_c-k+1}^{(B)} R_{b,n_c-k+1}^{*(B)} \tag{36}$$

$$D_{b,2k} = H_{b,k}^{*(B)} R_{b,k}^{(B)} - H_{b,n_c-k+1}^{(A)} R_{b,n_c-k+1}^{*(A)}. \tag{37}$$

Using a similar calculation in (12), (36) is rewritten as

$$D_{b,2k-1} = \underbrace{\left(\left|H_{b,k}^{(A)}\right|^2 + \left|H_{b,n_c-k+1}^{(B)}\right|^2\right) x_{b,2k-1}}_{\text{signal term}} + \underbrace{\left(\begin{array}{l} H_{b,k}^{*(A)} \sum_{m=1}^{n_c} Q\left(m+\varepsilon-k\right) H_{b,m}^{(B)} X_{b,m}^{(B)} \\ +H_{b,n_c-k+1}^{(B)} \sum_{m=1}^{n_c} Q\left(m-\varepsilon-(n_c-k+1)\right) H_{b,m}^{*(A)} X_{b,m}^{*(A)} \end{array}\right)}_{\text{Intra-blockICI}} + \underbrace{\left(\begin{array}{l} H_{b,k}^{*(A)} \sum_{\beta\neq b}^{N_b} \sum_{m=1}^{n_c} Q\left((\beta-b)\,n_c + m + \varepsilon - k\right) H_{\beta,m}^{(B)} X_{\beta,m}^{(B)} \\ +H_{b,n_c-k+1}^{(B)} \times \\ \sum_{\beta\neq b}^{N_b} \sum_{m=1}^{n_c} Q\left((\beta-b)\,n_c + m - \varepsilon - (n_c-k+1)\right) H_{\beta,m}^{*(A)} X_{\beta,m}^{*(A)} \end{array}\right)}_{\text{Inter-blockICI}} \tag{38}$$

where the second and third underlined terms denote the intra-block ICI and the inter-block ICI, respectively. We can express the signal power-normalized variances of intra-block ICI and inter-block ICI as follows: In order to numerically evaluate the ICI terms in (39) and (40), we randomly generate the fading coefficients $H_{b,k}^{(A)}$ and $H_{b,k}^{(B)}$ and data symbols and compute the expectations (39) and (40) over those values.

Fig. 9 illustrates the calculated powers of ICI terms according to the delay spread of selective multi-path fading channel. In this illustration, N is set to 256 and the subblock size n_c is set to 16. Regarding the multipath profile for generating the fading coefficients $H_{b,k}^{(A)}$ and $H_{b,k}^{(B)}$, the number of multi-paths is 8 and their delays are distributed uniformly in [0 T_{max}] where T_{max} is the delay spread. The guard interval is set to be larger than the delay spread T_{max}. The subcarrier spacing is set to 15kHz from LTE standard [19], i.e., OFDM symbol duration T is equal to $1/f_\Delta (= 1/15\text{kHz} = 0.67\mu sec)$. Each of four subplots in Fig. 9 corresponds to the cases with different subcarrier position within the subblock.

In Fig. 9, we found that as getting close to the band edge ($k = 1$) of the subblock, inter-block ICI becomes significant. On the other hand, getting close to the middle area ($k = n_c/2$), intra-block ICI is getting greater than inter-block ICI. Irrespective of the subcarrier position, ICI terms increase as delay spread increases. Especially, intra-block ICI shows the significant increase. This is because with larger delay spread, i.e., for the case of more selective fading, the flat fading assumption within the subblocks deteriorates more and thus, the self intra-block ICI cancellation property of the proposed scheme can be less exploited. Overall, however, the self intra-block ICI cancellation property still works quite well and contributes to the reduction of total ICI power level for wide range of delay spread except the very edge ($k = 1$) of the subblock. With high delay spread, the total ICI powers are even larger than the case with $n_c = 2$ which has the equivalent transmit signal structure as the conventional space frequency Alamouti coded OFDM. This implies that in order to guarantee the improvement over the conventional space frequency Alamouti coded OFDM, it is essential to properly set the subblock size n_c according to the considered channel selectivity. In other words, if the subblock size is not properly set according to the fading selectivity, the performance gain would not be guaranteed in severely selective fading environment.

The simulation results in the next section show that the optimal n_c is mainly determined by the delay spread (reciprocal to the coherent bandwidth) and relatively less sensitive to the other system parameters such as SNR or FO. Based on the extensive simulations over various channels of different delay spreads as shown in Fig. 13, we provide a simple and efficient decision rule for n_c as a function of delay spread in Fig. 14. In the next section, we will investigate the error rate performance of the proposed scheme in detail for the case when the subblock size is optimized according to the channel

$$\begin{aligned}
&\sigma^2_{(b,2k-1),\text{intra}} \\
&= \mathrm{E}\left[\frac{|\text{intra-blockICI}|^2}{|\text{signal term}|^2}\right] \\
&= \mathrm{E}\left[\frac{\left|H^{*(A)}_{b,k}\sum_{m=1}^{n_c} Q(m+\varepsilon-k)H^{(B)}_{b,m}X^{(B)}_{b,m}+H^{(B)}_{b,n_c-k+1}\sum_{m=1}^{n_c} Q(m-\varepsilon-(n_c-k+1))H^{*(A)}_{b,m}X^{*(A)}_{b,m}\right|^2}{\left|\left|H^{(A)}_{b,k}\right|^2+\left|H^{(B)}_{b,n_c-k+1}\right|^2\right|^2|x_{b,2k-1}|^2}\right],
\end{aligned} \tag{39}$$

$$\begin{aligned}
&\sigma^2_{(b,2k-1),\text{inter}} \\
&= \mathrm{E}\left[\frac{|\text{inter-blockICI}|^2}{|\text{signal term}|^2}\right] \\
&= \mathrm{E}\left[\frac{\left|H^{(A)*}_{b,k}\sum_{\beta\neq b}^{N_b}\sum_{m=1}^{n_c} Q((\beta-b)n_c+m+\varepsilon-k)H^{(B)}_{\beta,m}X^{(B)}_{\beta,m}+H^{(B)}_{b,n_c-m+k}\sum_{\beta\neq b}^{N_b}\sum_{m=1}^{n_c} Q((\beta-b)n_c+m-\varepsilon-(n_c-k+1))H^{*(A)}_{\beta,m}X^{*(A)}_{\beta,m}\right|^2}{\left|\left|H^{(A)}_{b,k}\right|^2+\left|H^{(B)}_{b,n_c-k+1}\right|^2\right|^2|x_{b,2k-1}|^2}\right].
\end{aligned} \tag{40}$$

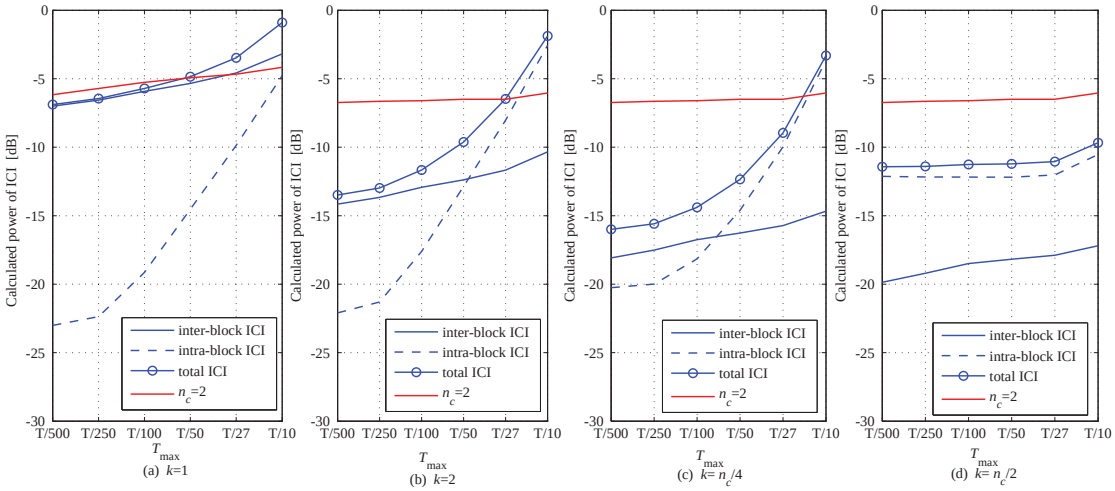

Fig. 9. Powers of ICI terms according to the delay spread for different subcarrier positions, $N = 256$ and $n_c = 16$.

selectivity.

IV. Performance Evaluation

A. Flat fading channel

In the flat fading channel, the proposed scheme is compared mainly with the results in the reference [1] which are referred to as *Xia's scheme*. The results reported by Li and Xia [2] were not included due to the very limited FO regions for acceptable performance and the poor data rate compared to the proposed scheme and Xia's scheme. The scheme reported by Choi [3] has a different baseline from the proposed scheme and Xia's scheme because its ICI-free performance is based on the critical assumption of perfect FO feedback to the TX sides. Therefore, the performance comparison with the scheme in the reference [3] is not appropriate.

Fig. 10 shows the simulated Bit Error Rate (BER) curves of the proposed scheme and Xia's scheme according to normalized FO ε in flat fading. The simulation parameters are set as those in [1]. The number of subcarriers N is set to 64 and each subcarrier is modulated by Quadrature Phase Shift Keying (QPSK). For fairness, the corresponding data rate is specified to the simulated BER curves of each system. According to the definition in [1], the data rate R_s is calculated as

$$R_s = \frac{N - N_v - N_u}{N - N_v}, \tag{41}$$

where N_v denotes the number of virtual subcarriers and N_u denotes the additional null subcarriers. In Xia's scheme, the cases with $N_v = 12$ and $N_u = 6$, 10 were considered as in [1]. Basically in the proposed scheme, $N_v = 0$ and $N_u = 4$ as explained at the end of the section III-A. For a unified number of virtual subcarriers with Xia's scheme in [1], the proposed scheme with $N_v = 12$ and $N_u = 4$ is also included. As done in Xia's scheme, we follow 802.11a standard [16] for the virtual subcarrier postions, i.e., the virtual subcarriers are located in 1st and 28th $\sim$ 38th subcarrier positions. The BERs of Xia's scheme deviate slightly from the ICI free case ($\varepsilon = 0$) when ε is relatively small. As ε increases, Xia's scheme degrades severely and needs to pay a substantial number of additional null subcarriers for compensation. On the other hand, the proposed scheme achieves almost ICI free performance for all ranges of FO and SNR. Hence,

the proposed scheme allows frequency synchronization erro between two distributed antennas even up to double (twice of) subcarrier spacing. This is beneficial especially to the recent OFDM-based systems, where the subcarrier spacing is getting smaller and thus, frequency synchronization between two distributed antennas is more difficult than the classical OFDM-based systems.

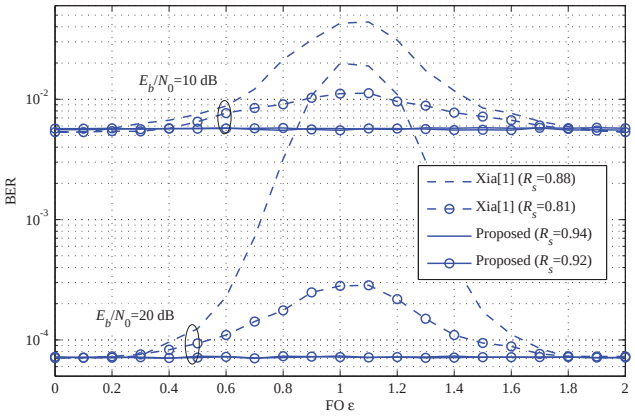

Fig. 10. BERs according to ε with $N = 64$, QPSK and $E_b/N_0 = 10$ dB and 20 dB.

Fig. 11 shows the simulated BER curves according to E_b/N_0 for various cases of N and ε when (N_v, N_u)=$(12, 10)$ and $(12, 4)$ for Xia's scheme and the proposed scheme, respectively. For a larger number of total subcarriers, i.e., $N = 256$, Xia's scheme degrades more significantly as FO ε increases compared to the case of $N = 64$. On the other hand, the proposed scheme achieves almost ICI free performance irrespective of N and ε. Moreover, the proposed scheme has higher data rate R_s (smaller number of null subcarriers) than that of the Xia's scheme.

Fig. 12 shows the simulated SER curves for the cases of 16 QAM, 64 QAM and 256 QAM with $N = 256$. Commonly for both of the proposed scheme and Xia scheme, the number of the additional null subcarriers N_u is set to 16, 44 and 96 for 16 QAM, 64 QAM and 256 QAM, respectively as determined in Fig. 5 and thus, data rates are the same for both schemes as well. The virtual subcarriers are not inserted, i.e., $N_v = 0$ for all the cases. The proposed scheme still achieves almost ICI free performance irrespective of ε for higher order QAM as observed in QPSK modulation. On the other hand, Xia's scheme degrades more severely as FO ε increases with higher order QAM compared to QPSK modulation. Summing up all the simulation results in flat fading channel, the proposed scheme consistently achieves the desired ICI cancellation property irrespective of the range of FO, the number of total subcarriers and the employed modulation schemes.

In addition to nearly ICI free performance, the proposed scheme requires quite less computational complexity compared to Xia's scheme. In Xia's scheme, one FFT operation and one matrix inversion of $N \times N$ Toeplitz matrix are performed. According to the typical methods, FFT operation requires $N\log_2 N$ multiplication and accumulation operations,

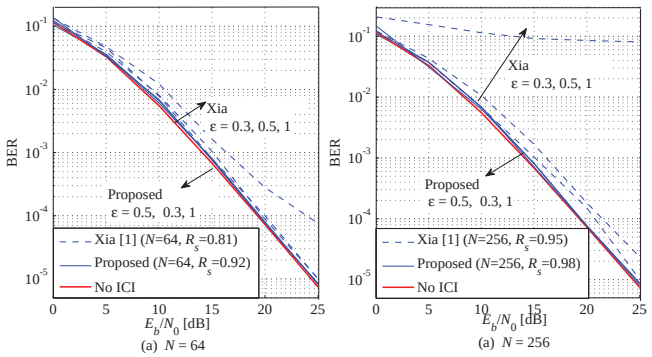

Fig. 11. BER curves for various N and ε with QPSK modulation.

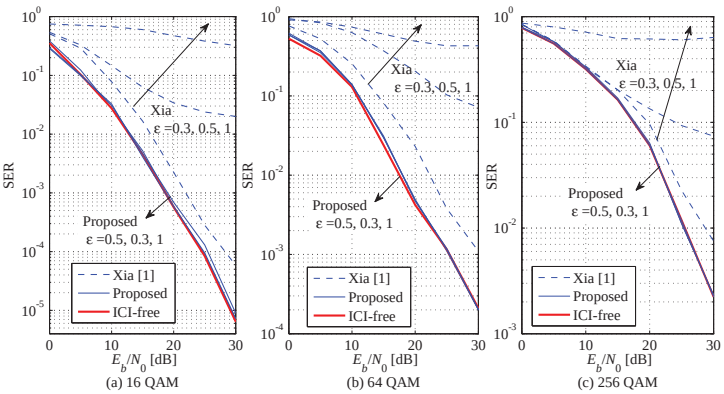

Fig. 12. SER curves for various ε according to E_b/N_0 with higher order QAM.

and the Toeplitz matrix inversions requires $N\log_2^2 N$ multiplication and accumulation operations . Therefore, total computation required by Xia's scheme is $(1+\log_2 N)N\log_2 N$ multiplication and accumulation operations. As for the proposed scheme, two FFT operations are performed without any other matrix operations and thus, the total computation is $2N\log_2 N$ multiplication and accumulation operations. Consequently, the proposed scheme saves multiplication and accumulation operations with a factor of $(1 + \log_2 N)/2$ compared to Xia scheme and thus, the computational complexity of the proposed scheme is significantly reduced compared to Xia scheme for typical range of N. Table II shows the the number of multiplications and accumulations for Xia's scheme and the proposed scheme.

TABLE II
THE NUMBER OF MULTIPLICATIONS AND ACCUMULATIONS OF XIA'S SCHEME AND THE PROPOSED SCHEME.

N	Xia	Proposed	Ratio(Proposed/Xia)
64	2,688	768	0.29
128	7,168	1,792	0.25
256	18,342	4,096	0.22
512	46,080	9,216	0.20
1,024	112,640	20,480	0.18
4,096	638,976	98,304	0.15

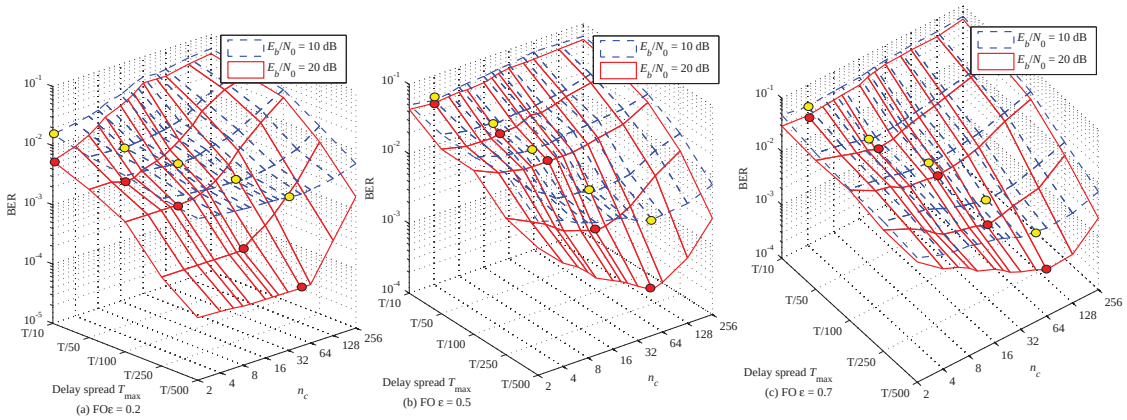

Fig. 13. BERs according to n_c for various E_b/N_0s, T_{max}s and εs.

B. Frequency selective fading channel or cases with practical timing offset between TX antennas

Consider the frequency selective fading channel, where the total subcarriers are divided into multiple subblocks in the proposed scheme as shown in Fig. 8. Within each subblock, the frequency reversal scheme is separately used without null subcarriers. The number of total subcarriers N is set to 256 to accommodate a larger variety of block sizes (number of subcarriers per block) n_cs. Regarding the multipath profile, the number of multi-paths is 8 and their delays are distributed uniformly in $[0\ T_{max}]$ where T_{max} is the delay spread. The guard interval is set to be larger than the delay spread T_{max}. The subcarrier spacing is set to 15kHz from LTE standard [19], i.e., OFDM symbol duration T is equal to $1/f_\Delta (= 1/15\text{kHz} = 0.67\mu sec)$.

Fig. 13 shows BERs of the proposed scheme according to n_c for various cases of the channel parameters, i.e., FO ε, SNR E_b/N_0 and delay spread T_{max}. At each curves (mesh lines) in function of n_c, the local minimum BER points are marked with the small circles. In order to clearly investigate functional relationship of optimal n_c on the channel parameters, the optimal n_cs corresponding to the all the local minimum BER points are plotted in Fig. 14. It is clear that the optimal n_c gradually decreases as T_{max} increases, i.e, as the fading becomes more frequency-selective. This is because ICI self-cancellation works based on flat fading condition over the subblocks and thus, we have to decrease the subblock bandwidth sufficiently enough to approximate the fading to be flat within the subblock bandwidth. The optimal n_c is invariant to E_b/N_0. Although the optimal n_c changes according to FO ε more or less, we note that the delay spread T_{max} is the most dominant factor to determine optimal n_c which ranges from 2 up to 64. This leads us to consider a simple and efficient decision rule for n_c as a function of delay spread only, which is specified as 'suboptimal' in Fig. 14.

Fig. 15 shows the BERs of the proposed scheme with the suboptimal n_c for various cases of the selective fading channels. For comparison, we include the case with $n_c = 2$ which corresponds to the conventional space frequency Alamouti code structure[3] and the case with fully optimized n_c. We note that the performance gap between the proposed scheme and the conventional code structure is substantial still in the selective channel. It is remarkable that even with the suboptimal n_c, the proposed scheme achieves almost the same performance with the fully optimum n_c. This implies that in order to achieve the desirable performance of the proposed scheme, we only have to measure delay spread and properly set n_c according to the rule shown in Fig. 14. In case of TDD (Time Division Duplex), delay spread can be also easily measured by using channel reciprocity between up and down links and thus, overall overhead for practical application is acceptable. As expected, the performance improvement over the conventional space frequency Alamouti code structure is relatively small for large delay spread (severely selective fading). Meanwhile, the performance improvement becomes significant as FO increases and the delay spread decreases.

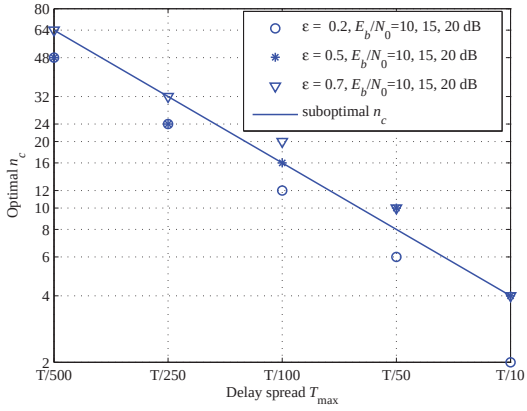

Fig. 14. Optimal n_c according to T_{max} and E_b/N_0 for several εs.

[3]We denote the proposed scheme with $n_c = 2$ by *conventional space frequency Alamouti code structure* because the proposed scheme with $n_c = 2$ is identical to the conventional scheme in the TX side. However, in the RX side, the proposed scheme performs two DFT operations while the conventional scheme performs single DFT operation tuned somewhere between the frequencies of two TX antennas. Therefore, the proposed scheme even with $n_c = 2$ still achieves ICI self-cancellation within each Alamouti code word and thus, the actual conventional scheme is worse than our reference in comparison denoted by *conventional space frequency Alamouti code structure*.

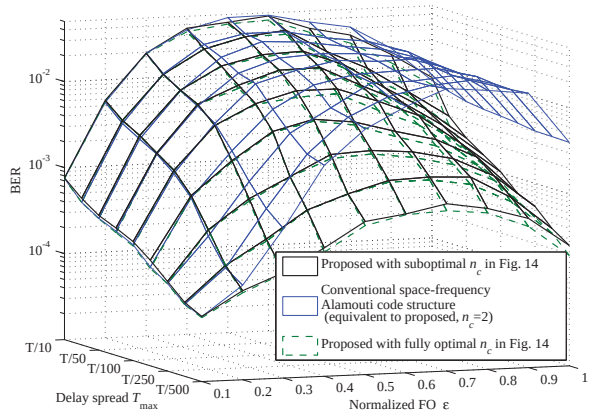

Fig. 15. BERs according to ε and T_{max} with $E_b/N_0 = 20$ dB.

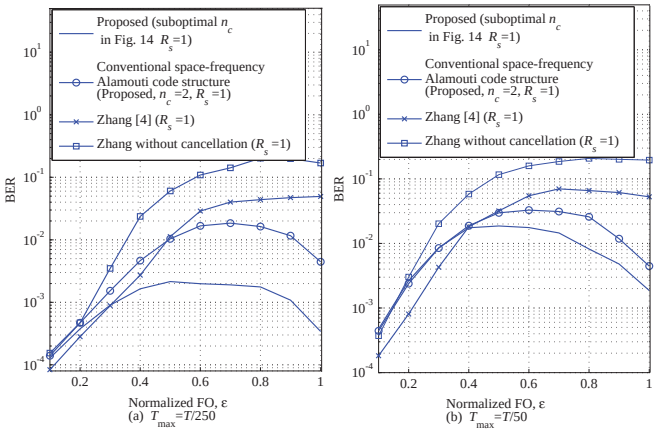

Fig. 16. BERs according to ε with QPSK, $N = 256$, subcarrier spacing = 15 kHz and the number of multi-paths = 8.

For accurate performance comparison, we cut three-dimensional BER surfaces in Fig. 15 at the delay spread $T_{max} = T/250$ and $T_{max} = T/50$ respectively and plot the corresponding sectional views in Fig. 16. Zhang's scheme [4] which has been proposed for the selective fading channel is simulated and its BER curves are also included in Fig. 16 for comparison. The BER performance of the proposed scheme gradually degrades as ε approaches 0.5, which is the worst case ε. Due to the non-constant fading coefficients within each subblock, the intra-block ICI self-cancellation error (summation of $I_{2k-1,1}$ in (32) and $I_{2k-1,4}$ in (33)) becomes larger as ε increases to 0.5. In addition, the ICI from the adjacent subblocks also becomes larger as ε increases to 0.5. This was not the case for the flat fading channel, where the proposed scheme achieves almost ICI-free performance irrespective of ε. Nevertheless, in the selective fading channel, the proposed scheme still achieves a meaningfully lower BER than the conventional space frequency Alamouti code structure ($n_c = 2$) and this improvement becomes significant in the mildly selective fading channels.

Compared to Zhang's scheme, the proposed scheme achieves significantly better performance in the large FO region. The error rate of Zhang's scheme degrades to the unacceptable level as FO increase. Meanwhile in the small FO region, Zhang's scheme works well and performs better than the proposed scheme. This is due to the fact that Zhang's scheme employs an additional cancellation step which requires high computation complexity. For fair comparison in terms of complexity, we simulated Zhang's scheme without the additional cancellation step and its BER curves are also included in Fig. 16, where we note that Zhang's scheme achieves severely worse performance than the proposed scheme even in small FO range.

Fig. 17 shows the BERs of the proposed scheme when there is timing offset (TO) between antennas A and B in the flat fading channel. The guard interval of OFDM symbol is assumed to be larger than TO. The reason for considering the flat fading channel is to decouple frequency selectivity by multipath fading and only to examine the equivalent frequency selectivity from timing offset. The TO is assumed to be within a few percentages of the OFDM symbol duration considering the practical ranging operation. Similar to the case of the selective fading channel, the proposed scheme without subblock partitioning ($n_c = N$) shows poor BER performance because ICI cancellation condition, i.e., constant fading coefficient within the block is severely destroyed. In addition, for the case of $n_c = 2$, which is equivalent to the conventional space frequency Alamouti code structure, the BER performance deteriorates as ε increases. On the other hand, properly selecting n_c in the middle, the proposed scheme achieves a much lower BER than those of the two extreme cases of $n_c = 2$ and N. A comparison of the results between TO $= 1\%$ and 3% of the OFDM symbol duration reveals a decrease in the optimal n_c as TO increases. This is because the equivalent frequency selectivity increases with increasing TO and the subblock size needs to be decreased for constant fading approximation. In the practical case when the TX cannot adjust n_c according to TO, n_c should be chosen so that it minimizes the BER of the worst case situation.

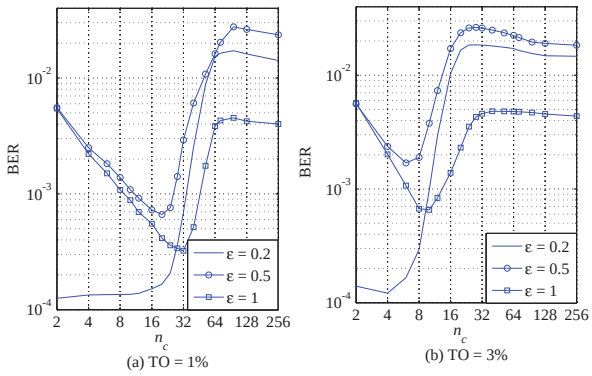

Fig. 17. BERs according to n_c for TO $= 1\%$ and 3% of the OFDM symbol duration with $N = 256$, QPSK and E_b/N_0=20dB in the flat fading channel.

V. Conclusions

The ICI self-cancellation scheme is proposed for Alamouti coded OFDM for distributed antenna systems. The results

of the derivation and simulation show that in flat fading channels, the ICI component due to FO between the TX antennas is drastically cancelled during the combining process. In addition, an extended modification of the proposed scheme is provided for selective fading channel or cases with timing offset between TX antennas. In three aspects, i.e., complexity, data rate and BER performance, the proposed scheme is found to be a promising solution for distributed Alamouti coded OFDM systems with FO between TX antennas.

APPENDIX
PROOF OF EQUATION (14)

Let $x + y = t$, then the integral in (14) is calculated as follows :

$$\begin{aligned}&\int_0^\infty \int_0^\infty e^{-(x+y)} \frac{xy}{(x+y)^2}\ \mathrm{d}x\ \mathrm{d}y \\ &= \int_0^\infty \int_y^\infty \frac{e^{-t}}{t^2}(t-y)y\ \mathrm{d}t\ \mathrm{d}y \\ &= \int_0^\infty \left[y \int_y^\infty \frac{e^{-t}}{t}\ \mathrm{d}t - y^2 \int_y^\infty \frac{e^{-t}}{t^2}\ \mathrm{d}t \right]\ \mathrm{d}y. \quad \text{(A-1)}\end{aligned}$$

Using the integral formulas in [20] $\int_y^\infty \frac{e^{-t}}{t}\ \mathrm{d}t = -\mathrm{E}_i(-y)$ where $\mathrm{E}_i(x)$ denotes exponential integral function and $\int_y^\infty \frac{e^{-t}}{t^2}\ \mathrm{d}t = \mathrm{E}_i(-y) + \frac{e^{-y}}{y}$ and substituting these into (A-1),

$$\begin{aligned}&\int_0^\infty \int_0^\infty e^{-(x+y)} \frac{xy}{(x+y)^2}\ \mathrm{d}x\ \mathrm{d}y \\ &= -\int_0^\infty y^2 \mathrm{E}_i(-y)\ \mathrm{d}y - \int_0^\infty y\mathrm{E}_i(-y)\ \mathrm{d}y - \int_0^\infty y e^{-y}\ \mathrm{d}y,\end{aligned}$$

Using another integral formula in [20] $\int_0^\infty y^k \mathrm{E}_i(-y)\ \mathrm{d}y = -\frac{\Gamma(k+1)}{k+1}$,

$$\begin{aligned}&\int_0^\infty \int_0^\infty e^{-(x+y)} \frac{xy}{(x+y)^2}\ \mathrm{d}x\ \mathrm{d}y \\ &= \frac{\Gamma(3)}{3} + \frac{\Gamma(2)}{2} - 1 \\ &= \frac{1}{6}\ .\end{aligned}$$

REFERENCES

[1] H. Wang, X.-G. Xia, and Q. Yin, "Distributed space-frequency codes for cooperative communication systems with multiple carrier frequency offsets," *IEEE Trans. Wirel. Communs.*, vol. 8, no. 2, pp. 1045–1055, Feb. 2009.
[2] Z. Li and X.-G. Xia, "An Alamouti coded OFDM transmission for cooperative systems robust to both timing errors and frequency offsets," *IEEE Trans. Wirel. Communs.*, vol. 7, no. 5, pp. 1839–1844, May 2008.
[3] K. Choi, "Inter-carrier interference-free Alamouti-coded OFDM for cooperative systems with frequency offsets in non-selective fading environments," *IET Communs.*, vol. 5, no. 15, pp. 2125–2129, Oct. 2011.
[4] Y. Zhang, "Multiple CFOs compensation and BER analysis for cooperative communication systems," in *Proc. IEEE WCNC'09*, pp. 1–6, Apr. 2009.
[5] T. Lu, H. Lin, and T. Sang, "An SFBC-OFDM receiver to combat multiple carrier frequency offsets in cooperative communications," in *Proc. IEEE PIMRC 2010 Symp.*, pp. 899–904, Sep. 2010.
[6] F. Tian, X.-G. Xia, and P. C. Ching, "Equalization in space-frequency coded cooperative communication system with multiple frequency offsets," in *Proc. IEEE ISSCS* vol. 2, pp. 1–4, Jul. 2007.
[7] W. Zhang, W. Humming, Q. Yin, and W. Wang, "Space frequency code for cooperative communications with both timing errors and carrier frequency offsets," *IEICE Trans. Communs.*, vol. E93-B, no. 12, pp. 3305–3508, Dec. 2010.
[8] Q. Huang, M. Ghogho, and J. Wei, "Data detection in cooperative STBC-OFDM systems with multiple frequency offsets," *IEEE Signal Proc. Letters*, vol. 16, no. 7, pp. 600–603, Jul. 2009.
[9] K. Lee and D. Williams, "A space-frequency transmitter diversity technique for OFDM systems," in *Proc. IEEE GLOBECOM '00*, vol. 3, pp.1473–1477, Nov. 2000.
[10] F. Ng and X. Li, "Cooperative STBC-OFDM transmissions with imperfect synchronization in time and frequency," in *Proc. 39th Asilomar Conf. Signals, Syst. and Computers*, pp. 524–528, Oct. 2005.
[11] S. M. Alamouti, "A simple transmitter diversity scheme for wireless communications," *IEEE J. Sel. Areas Communs.*, vol. 16, no. 8, pp. 1451–1458, Oct. 1998.
[12] P. Dharmawansa, N. Rajatheva, and H. Minn, "An exact error probability analysis of OFDM systems with frequency offset," *IEEE Trans. Communs.*, vol. 57, no. 1, pp. 26–31, Jan. 2009.
[13] Y. Yao, and X. Dong, "Multiple CFO mitigation in amplify-and-forward cooperative OFDM transmission," *IEEE Trans. Commun.*, vol. 60, no. 12, pp. 3844–3854, Dec. 2012.
[14] F. Tian, P. C. Ching, and X. G. Xia "A simple ICI mitigation method for a space-frequency coded cooperative communication system with multiple CFOS," in *Proc. IEEE ICASSP 2008*, pp. 3253–3256, Mar. 2008.
[15] S. Aghajeri, M. Gholami, and H. Nikopoor, "Blind sampling clock adjustment in OFDM power line communication," in *Proc. IEEE ISSPA 2007*, pp. 1–4, Feb. 2007.
[16] IEEE 802.11 Working Group, "Wireless LAN Medium Access Control (MAC) and Physical Layer (PHY) Specification," 1997.
[17] V. Erceg, L. J. Greenstein, S. Y. Tjandra, S. R. Parkoff, A. Gupta, B. Kulic, A. A. Julius, and R. Bianchi, "An empirically based path loss model for wireless channels in suburban environments," *IEEE J. Sel. Areas Communs.*, vol. 17, no. 7, pp. 1205–1211, Jul. 1999.
[18] E. Foutekova, P. Agaypong, and H. Haas, "Channel asymmetry and random time slot hopping in OFDMA-TDD cellular networks," in *Proc. VTC Spring 2008*, pp. 1671–1675. May 2008.
[19] S. Sesia, I. Toufik, and M. Baker, Eds., *LTE: The UMTS Long Term Evolution.* John Wiley and Sons, 2009.
[20] I. Gradshteyn and I. Ryzhik, *Table of Integrals, Series, and Products,* 5th ed., New York: Academic, 1994.

PLACE PHOTO HERE

Bong-seok Kim received his B.S. degree in department of electronics engineering in 2006 and the M.S. and Ph.D. degrees in department of information and communications Engineering of Yeungnam university, Korea, in 2009 and 2014, respectively. He is currently working in Creative human resource development team for ICT-based smart devices of Brain Korea 21 Plus as a research staff. His current interests include physical layer for 5G and beyond communication systems.

PLACE PHOTO HERE

Kwonhue Choi received his B.S. M.S. and Ph.D. degrees in electronic and electrical engineering from POSTECH, Korea, in 1994, 1996 and 2000, respectively. From 2000 to 2003, he has been with ETRI, Korea as a senior research staff. In 2003, he joined Yeungnam University, Korea. From September 2008 to Agust 2009, he was a visiting professor at Oregon State University, USA. Currently he is a full professor at department of information and communications, Yeungnam University. His research area includes efficient multiple access, diversity schemes under fwireless fading channels and cooperative communications for 5G and beyond systems.